Thermo-Hydraulic Performance of Microchannel Heat Sinks with Square Pin-Fin Geometries: A Numerical Investigation

1st Ashraf Morsi
Mechanical Engineering Department
Faculty of Engineering
Alexandria University
Alexandria, Egypt
ORCID: 0009-0003-0337-3507

2nd Mohammed Abdel Razzaq
Texas Institute for Electronics
The University of Texas at Austin
Austin, TX, USA
ORCID: 0009-0000-0912-6927

3rd Youssef Khalid
Mechanical Power Department,
Faculty of Engineering
Cairo University
Cairo, Egypt
ORCID: 0009-0000-7191-4916

4th Mohamed Naser
Faculty of Engineering
Alexandria University
Alexandria, Egypt
ORCID: 0009-0008-4600-3502

5th Mohamed Elkholy
Mechanical Power Engineering
Menoufia University
Menoufia, Egypt
ORCID: 0009-0004-3033-894X

6th Ibrahim Elhagali
Power and Wide-Band-Gap
Electronics Research Laboratory
(POWERlab), EPFL
Lausanne, Switzerland
ORCID: 0000-0003-3117-0232

*7th Osama Maklad
School of Engineering, University of Greenwich, London, UK
Mechanical Power Engineering Department, Mansoura University
Mansoura, Egypt
ORCID: 0000-0001-6893-2654
*Corresponding author: o.maklad@gre.ac.uk

Abstract - **The continued rise in power density of modern electronic devices demands compact cooling solutions capable of dissipating extreme heat fluxes. This paper presents a three-dimensional computational fluid dynamics (CFD) investigation of the thermo-hydraulic performance of a multi-inlet microchannel heat sink (MCHS) incorporating square pin-fin arrays, with a 25% propylene glycol-water mixture (PG25) as the working fluid. A five-inlet manifold configuration is adopted to improve flow uniformity, and seven optimisation phases are systematically evaluated: five-inlet, five-inlet with square pins, chamfered pins (10%, 20%, 30%), cut square pins, filleted square pins, aspect-ratio-modified pins with cut-through holes, a novel high-performance design, and a fin-removal strategy. The base case (five-inlet with square pins) achieves a heat transfer coefficient (HTC) of 26,452 W/m²K at a pressure drop of 128.5 Pa and a pumping power of 0.001646 mW/mm². Among the configurations studied, the novel design (Novel 1) achieves the highest HTC of 41,975 W/m²K, representing a 40.2% improvement over the base case, albeit at a significantly elevated pumping power. Chamfered pins provide progressive hydraulic relief with a modest thermal trade-off, while the aspect-ratio modification with cut-through holes delivers a 5.1% HTC improvement with moderate hydraulic cost. The results demonstrate that geometric optimization can yield substantial performance improvements and provide guidelines for the design of high-performance microchannel cold plates.**

Keywords: Micro-channel heat sink; thermal management; pin fins; computational fluid dynamics (CFD); electronic cooling; pressure drop; conjugate heat transfer; Nusselt number.

I. INTRODUCTION

In recent decades, the semiconductor industry has largely followed the trajectory predicted by Moore [1], where the continuous miniaturization of electronic components has led to an exponential increase in transistor density. This rapid densification has resulted in a critical challenge: the generation of extreme heat fluxes that conventional air-cooling methods can no longer manage effectively [2,3]. Efficient thermal management has become a primary bottleneck in the design of high-performance devices, as operating temperatures directly correlate with component reliability and lifespan [4]. Consequently, there is an urgent demand for compact, high-capacity cooling solutions capable of dissipating these elevated heat loads [2,5].

To address these thermal challenges, Tuckerman and Pease [6] introduced the concept of the Micro-channel Heat Sink (MCHS). By utilizing channels with hydraulic diameters in the micrometer scale, MCHS devices achieve a significantly higher heat transfer surface area-to-volume ratio compared to macro-scale heat exchangers. Over the years, MCHS has established itself as a robust solution for cooling high-heat-flux devices, including laser diode arrays and concentrated photovoltaic cells [7]. However, as heat dissipation requirements continue to rise, relying solely on simple, straight rectangular microchannels is often insufficient due to the development of thick thermal boundary layers that impede heat transfer.

To further augment the thermal performance of MCHS, researchers have investigated various passive enhancement techniques, which typically involve modifying the channel geometry to disrupt flow and break the thermal boundary layer [8,9]. Among these techniques, the integration of pin fins and ribs into the flow path has proven highly effective.

Studies have shown that pin fins not only increase the available surface area but also induce fluid mixing and redevelop the thermal boundary layer. Vasilev et al. [10] and Alfellag et al. [11] demonstrated that varying the shape and arrangement of these pins—from circular to oval and solid/slotted designs—can dramatically alter the thermo-hydraulic performance. However, these geometric modifications often introduce a trade-off: the associated pressure drop can increase significantly, requiring higher pumping power [12]. Therefore, optimizing geometric parameters, such as fin height and spacing, is crucial. Recent research [13,14] has highlighted that the proximity of pins to the channel sidewalls and their height relative to the channel depth are critical factors in balancing heat transfer enhancement with hydraulic resistance.

While experimental validation remains important, the fabrication of complex micro-geometries using techniques like deep reactive ion etching or laser ablation is expensive and time-consuming [15]. Numerical modeling has thus become an indispensable tool for exploring a wide design space. Recent computational studies [16,17] have successfully utilized Computational Fluid Dynamics (CFD) to predict flow patterns and temperature distributions in complex microchannels with high accuracy. These numerical approaches allow for the detailed visualization of local flow structures—such as secondary flows and vortices—that are difficult to capture experimentally but are essential for understanding the mechanism of heat transfer enhancement [18].

While the utility of pin fins is well-established, two major challenges in practical application remain: mitigating flow maldistribution across the heat sink to avoid localized hotspots, and further optimizing the pin-fin geometry to maximize performance without an excessive increase in pumping power. To address these, the present study introduces and numerically investigates a five-inlet manifold configuration to enhance flow uniformity across the heat sink base. The primary focus is on square pin-fin arrays, a geometry known for its strong flow separation and turbulence characteristics. We systematically explore modifications to this base geometry, specifically evaluating the impact of increasing fin thickness and introducing minor boundary modifications (e.g., fillets and cut-through pins). Using Computational Fluid Dynamics (CFD), the objectives of this work are to: 1) quantitatively compare the thermo-hydraulic performance of single-inlet versus five-inlet cold plate designs; 2) analyse the sensitivity of the performance to geometric parameters such as fin thickness; and 3) identify the optimized pin-fin configuration, such as the novel cut-through pin design, that yields the most favourable performance evaluation criterion (PEC) for high-heat-flux electronic cooling applications.

II. Physical Model and Cooling System

A. Cooling System Description

Fig. 1 shows the proposed system-level integration of the investigated cold plate within a closed liquid-cooling loop; the schematic explains the system context and boundary conditions and does not represent an experimental setup. Heat generated by the GPU die is conducted through a thermal interface material (TIM) into the copper cold plate, whose wetted side carries the square pin-fin microchannel array. The PG25 coolant is distributed over the array by a five-inlet manifold, collects the dissipated heat, and rejects it to the ambient in a radiator before returning to the reservoir and pump. The present study resolves the cold plate and its internal flow; the remaining loop components define the boundary conditions (coolant supply temperature and flow rate) but are not modeled explicitly.

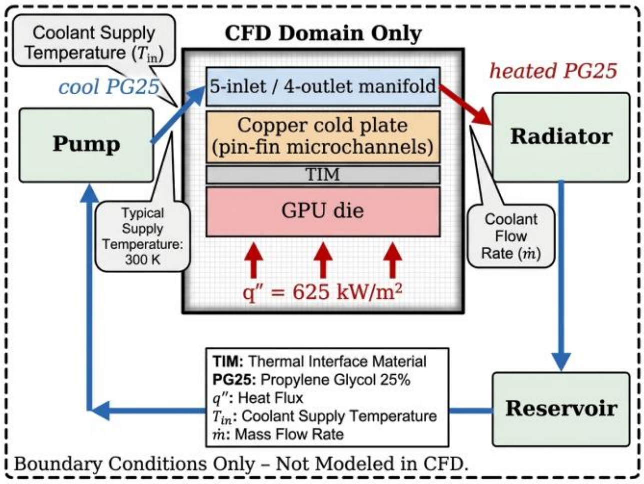

Fig. 1. Proposed system-level integration of the five-inlet microchannel cold plate within a closed liquid-cooling loop. Only the cold plate is included in the CFD domain; the GPU, TIM, pump, radiator, and reservoir are shown for context.

B. Heat Sink Geometry

The heat sink is a copper microchannel cold plate featuring an array of 200 μm × 200 μm square pin fins, designed for a dissipation rate commensurate with a modern high-power component such as the H200 GPU. To address the flow maldistribution and localized thermal non-uniformity identified in the preliminary single-inlet study, the cold plate employs the five-inlet, four-outlet manifold configuration shown in Fig. 2, in which each inlet and its consecutive outlet are spaced 3.5 mm apart. The five inlets subdivide the wetted footprint, sized for a GPU logic area of 800 mm², represented as an assumed 28.28 × 28.28 mm square for determining the total heat load, into shorter parallel flow paths, which both equalizes the flow distribution over the pin-fin array and reduces the streamwise pressure build-up. The coolant passages between the fins are 0.20 mm wide and 2.00 mm deep, giving a channel aspect ratio of 10. The CFD model itself resolves one representative repeating unit cell of this array rather than the complete cold plate, as described in Section III-A. The principal geometric parameters of the cold plate and of the three optimisation phases are compiled in Table I.

TABLE I. Geometric Parameters of the Five-Inlet Microchannel Cold Plate

Parameter	Value
GPU logic (heated) area	800 mm² (28.28 × 28.28 mm assumed square; sets the total heat load)
CFD computational domain	one repeating unit cell
Cold-plate thickness	4 mm
Microchannel height × width	2.00 mm × 0.20 mm
Channel aspect ratio	10
Unit-cell heated area, Aref	0.70 mm²
Pin width (square cross-section)	0.20 mm (200 μm)
Baseline pin height	2 mm

Streamwise / transverse pitch	0.6 mm
Number of pin fins	8
Manifold configuration	5 inlets / 4 outlets
Inlet-to-consecutive-outlet spacing	3.5 mm
Inlet / outlet dimensions	0.5 x 0.2 mm^2
Fillet radii	0.03 mm, 0.05 mm
Alternating-height increments	+10%, +20%, +30%
Cut-through-hole width / diameter	40% of pin height
Cut-through-hole position	transverse, through the small, big, or both fin groups

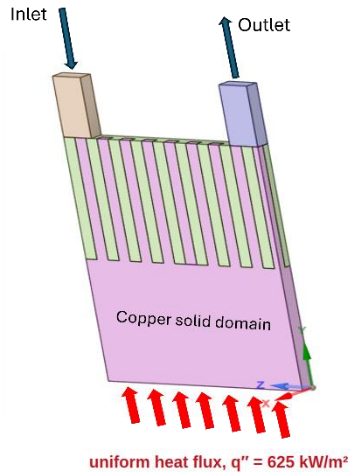

Fig. 2. Geometry of the five-inlet square pin-fin heat sink.

C. Materials and Working Fluid

The heat sink material is high-conductivity copper, whose large thermal conductivity spreads the heat rapidly along the fins and sustains their effectiveness. The working fluid is a 25% propylene glycol-water mixture (PG25), selected for its high specific heat capacity together with the anti-freeze and anti-corrosion characteristics required for industrial reliability. The thermophysical properties used in the simulations are listed in Table II; all properties are treated as constant.

TABLE II. THERMOPHYSICAL PROPERTIES OF THE HEAT SINK AND WORKING FLUID

Material	Property	Symbol	Value	Unit
Copper	Density	ρ	8960	kg/m³
	Specific heat	cp	385	J/(kg·K)
	Thermal conductivity	k	401	W/(m·K)
PG25	Density	ρ	1025.2	kg/m³
	Specific heat	cp	3955	J/(kg·K)
	Dynamic viscosity	μ	0.0022	Pa·s
	Thermal conductivity	k	0.472	W/(m·K)
	Prandtl number	Pr	18.43	–

D. Computational Model and Assumptions

The computational model solves for the conjugate heat transfer within the combined solid and fluid domains. The numerical analysis is based on several simplifying assumptions to define the limits of the simulation: the system is modeled under steady-state operating conditions, and the flow regime is assumed to be laminar throughout the domain. The coolant is treated as an incompressible and Newtonian fluid with constant thermophysical properties. Furthermore, viscous dissipation terms in the energy equation are neglected. The simulation utilizes a simplified 2D model of the flow and heat transfer. Under these conditions, the set of conservation equations solved includes the Continuity, Momentum, and Energy equations for both the fluid and solid domains.

III. NUMERICAL MODEL

A. Computational Domain and Assumptions

The three-dimensional computational domain comprises the three-dimensional PG25 fluid domain and the three-dimensional copper solid domain, coupled at all wetted surfaces to resolve the three-dimensional conjugate heat transfer; Fig. 3 shows a mid-plane section through the domain with the applied boundary conditions. The domain represents a repeating unit cell of the pin-fin array with a heated base area of 0.70 mm²—not the complete 28.28 × 28.28 mm cold plate—and the lateral symmetry boundaries exploit this periodicity; the reported flow rate and pumping power refer to this unit cell. The numerical analysis rests on the following assumptions: the system operates at steady state; the flow regime is laminar throughout the domain, as confirmed by the inlet Reynolds number; the coolant is an incompressible, Newtonian fluid with constant thermophysical properties; viscous dissipation in the energy equation is neglected; and buoyancy effects are not considered. Because the flow is laminar, the flow structures discussed in this paper—separation, recirculation, and secondary vortices—are steady laminar features.

B. Governing Equations

Under the stated assumptions, the conservation equations for mass (1), momentum (2), and energy (3) are solved over the three-dimensional fluid domain, while heat conduction is solved in the three-dimensional solid domain:

$$\frac{\partial \rho}{\partial t} + \nabla \cdot (\rho \vec{U}) = 0 \quad (1)$$

$$\rho \frac{D\vec{U}}{Dt} = -\nabla p + \rho \vec{g} + \mu \nabla^2 \vec{U} \quad (2)$$

$$\frac{\partial(\rho E)}{\partial t} + \nabla \cdot (\rho E u) = \nabla \cdot (k \nabla T) - \nabla \cdot (p u) + S_h \quad (3)$$

C. Boundary Conditions

The thermal and hydraulic operating conditions replicate the design point of the target component. The inlet is specified as a mass-flow inlet with a flow rate of 9×10^{-6} kg/s per computational unit cell—not for the entire cold plate—and a fixed coolant temperature of Tin = 300 K. The outlet is a zero-gauge pressure outlet. A uniform heat flux of q″ = 625 kW/m² is applied to the base of the cold plate, corresponding to a total heat load of 500 W over the 800 mm² GPU logic area and representing the heat generation of the electronic component after spreading through the TIM. The front, back, and lateral external walls are treated as symmetry boundaries; all wetted walls are no-slip; and the copper-PG25 interface is a coupled boundary that enforces continuity of temperature and heat flux for the conjugate problem (Fig. 3).

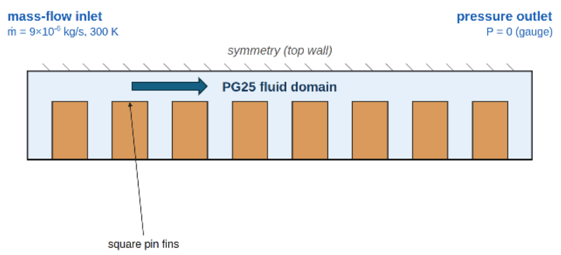

Fig. 3. Computational domain and boundary conditions, shown as a mid-plane section through the three-dimensional domain. The copper solid and PG25 fluid domains are coupled at the wetted surfaces.

D. Performance Parameters

Hydraulic performance is evaluated through the pressure drop (4), defined as the difference between the mass-weighted average pressures at the inlet and outlet, and through the total pumping power (5), in watts, obtained by multiplying the pressure drop by the volumetric flow rate:

$$\Delta P = P_{in} - P_{out} \tag{4}$$

$$W_p = V \Delta P \tag{5}$$

The optimisation results are reported as the specific pumping power (6), the total pumping power normalized by Aref = 0.70 mm², the heated area of the computational unit cell, and expressed in mW/mm²; with this normalization, the base-case total pumping power of Table III corresponds to the reported specific value of 0.00161 mW/mm². The grid-independence study of Section III-F reports the total pumping power in watts.

$$W''_p = W_p / A_{ref} \tag{6}$$

Thermal performance is evaluated through the heat transfer coefficient (7), defined with the applied base heat flux and the fluid inlet temperature as the reference so that it constitutes a global, geometry-independent metric, and through the fin efficiency (8), the ratio of the actual to the maximum possible fin heat transfer:

$$h = \frac{q''}{T_{chip} - T_{in}} \tag{7}$$

$$\eta_{fin} = \frac{Q_{fin}}{Q_{fin,max}} \tag{8}$$

With this definition of h, the area-specific thermal resistance of the cold plate follows directly as its reciprocal, (9); for the base case it amounts to 3.78 × 10⁻⁵ m²K/W. Because (9) carries no independent information, the results are reported in terms of the HTC, the heated-surface temperature, the pressure drop, and the pumping power.

$$R''_{th} = (T_{chip} - T_{in})/q'' = 1/h \tag{9}$$

E. Solver and Numerical Procedure

The governing equations were solved with the finite-volume solver ANSYS Fluent v19.2 in steady, pressure-based mode. The laminar viscous model was used, consistent with the inlet Reynolds number.

The pressure-velocity coupling method, discretization schemes, convergence criteria, iteration counts, and computational hardware are compiled in the Remaining Author Inputs list pending confirmation by the authors.

F. Mesh and Grid Independence

A grid independence study was conducted using two three-dimensional meshes in which only the resolution was varied: a coarse mesh with a 0.03 mm element size (approximately 703,000 elements) and a fine mesh with a 0.02 mm element size (approximately 2,000,000 elements); geometry, physical models, boundary conditions, and solver settings were identical. The comparison in Table III shows that the pressure drop and total pumping power vary by less than 3%, while all thermal and fin-related quantities differ by less than 0.5%, confirming that the solution is effectively grid independent. The 0.03 mm mesh was therefore selected for the parametric optimisation campaign as the best balance between accuracy and computational cost, reducing the element count by approximately 65% relative to the fine mesh. Table III reports the dedicated mesh-comparison runs; the optimisation sections that follow use the final baseline dataset, which is why the baseline values quoted in Section V differ marginally from the tabulated mesh-study values. Fig.4 shows the 3D mesh overview and near-fin refinement close-up.

TABLE III. GRID INDEPENDENCE STUDY

Quantity	0.03 mm (703k elem.)	0.02 mm (2.0M elem.)	Diff. (%)
Pressure drop (Pa)	128.5	131.9	2.6
Total pumping power (W)	1.13×10^{-6}	1.16×10^{-6}	2.4
Source temperature (K)	323.63	323.67	0.01
Fluid avg. temperature (K)	309.8	309.9	0.03
HTC (W/m²K)	26,452	26,405	0.18
Fin efficiency (%)	77.77	77.67	0.13

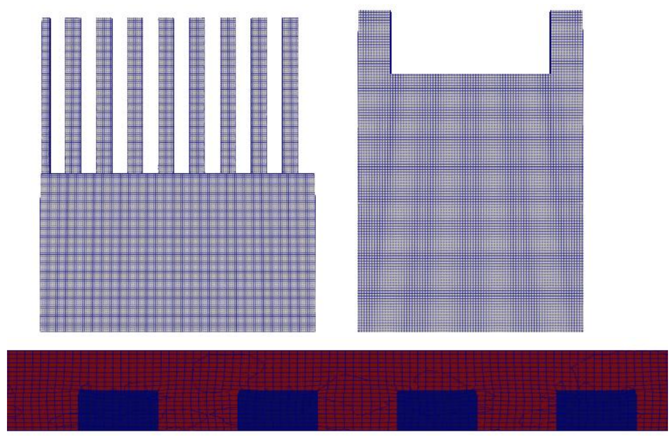

Fig. 4. 3D mesh overview and near-fin refinement close-up.

IV. Optimisation Strategy

The optimisation campaign was organized sequentially, as summarized in Fig. 4. Each phase isolates a single family of geometric parameters so that the observed change in performance can be attributed unambiguously to one physical mechanism. These are organized into the following categories:

1. Base case: Five Inlets with Square Pins, the control case against which all modifications are measured.
2. Pin shape modifications: Cut Square Pins (material removed from pin body) and Filleted Square Pins (fillet radii at the pin root).
3. Chamfer study: Chamfer at 10%, 20%, and 30%, progressive corner chamfering of the square pins.
4. Aspect ratio with cut-through: Modified pin aspect ratio combined with transverse cut-through holes.
5. Novel design (Novel 1): A high-performance configuration combining multiple geometric enhancements.
6. Fin removal: Strategic removal of selected fins to reduce flow blockage

This one-factor-at-a-time strategy is also a limitation: it cannot capture interactions between the parameter families and does not guarantee a global optimum; a formal multi-objective optimisation over the combined design space is identified as future work in Section VI.

All simulations were performed at a single operating point (unit-cell mass flow rate of 9×10^{-6} kg/s, inlet temperature of 300 K, and base heat flux of 625 kW/m²) because the study targets geometry optimisation at the design operating condition of the electronic component; the geometric ranking established here applies to that condition, and the sensitivity of the ranking to Reynolds number and heat load is left for future work.

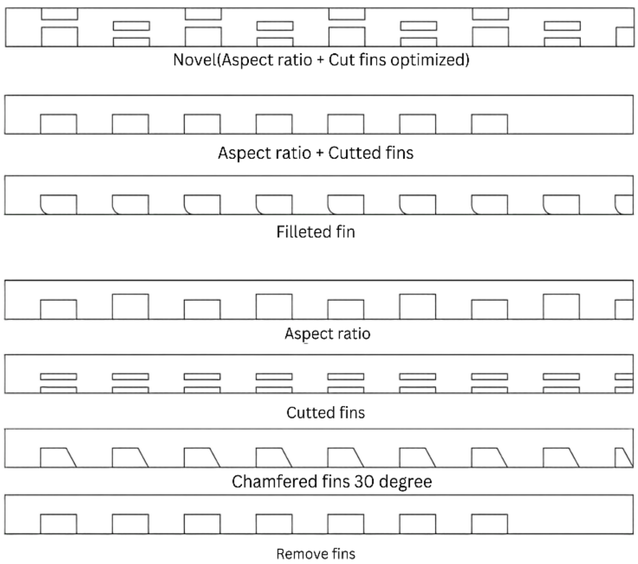

Fig. 4. *Overview of the investigated geometric configurations.*

V. Results and Discussion

This section presents the thermal and hydraulic performance of the baseline square pin-fin configuration, followed by the three optimisation phases explored in this study: fillet radii, alternating pin heights, and transverse cut-through holes.

A. Reference Configurations

Two reference configurations were simulated to establish performance baselines. The single-inlet configuration achieves an HTC of 32,740 W/m²K with a heater surface temperature of 322.09 K, but at a very high pressure drop of 1710.91 Pa and a pumping power of 0.0216 mW/mm². The five-inlet configuration (without pin fins) delivers a slightly higher HTC of 33,133 W/m²K at a dramatically reduced pressure drop of 231.80 Pa, with a pumping power of 0.0029 mW/mm² — representing a 86.6% reduction in pumping power compared to the single inlet. The five-inlet manifold design effectively distributes the flow, reducing the path length and the associated friction losses while maintaining comparable thermal performance.

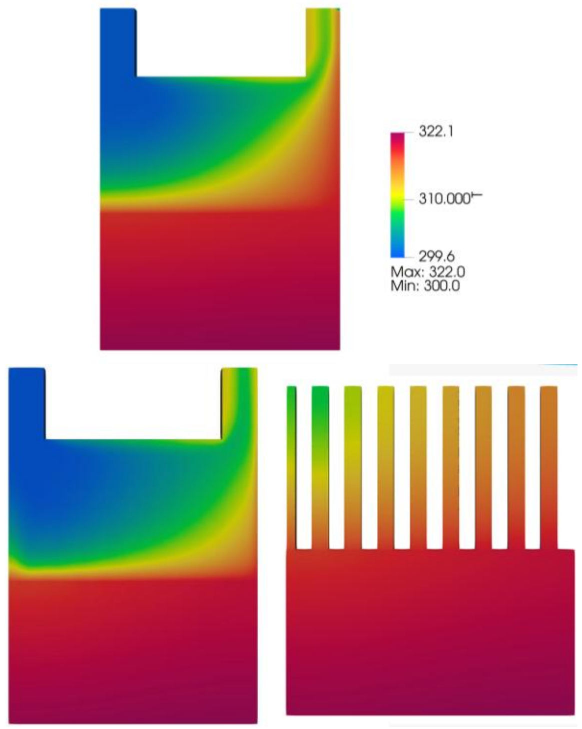

Fig. 5. Temperature distribution for the five-inlet configuration with and without the pin fins. The top is the case with no fins.

B. Base Case: Five Inlets with Square Pins

The base case features a uniform array of 200 µm × 200 µm square pin fins within the five-inlet manifold. It achieves an HTC of 29,950 W/m²K with a heater surface temperature of 323.87 K and a pressure drop of 131.21 Pa. The specific pumping power is 0.001646 mW/mm². Compared to the five-inlet reference (without pins), the addition of square pins reduces the HTC by 9.6% but also reduces the pressure drop by 43.4%, indicating that while the pins disrupt the flow and add form drag locally, the manifold-level flow redistribution leads to a net reduction in overall pressure loss. The pin fins serve as extended surfaces that conduct heat from the base into the fluid, but the sharp corners of the square pins generate stagnation zones and recirculating wakes that limit the thermal performance. These observations motivate the geometric modifications explored in the subsequent sections.

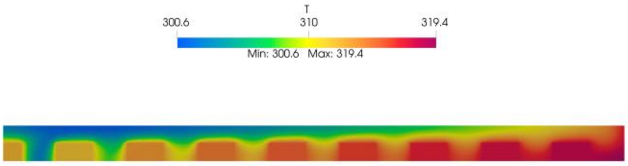

Fig. 6. Mid-plane temperature distribution for the base case (five inlets with square pins).

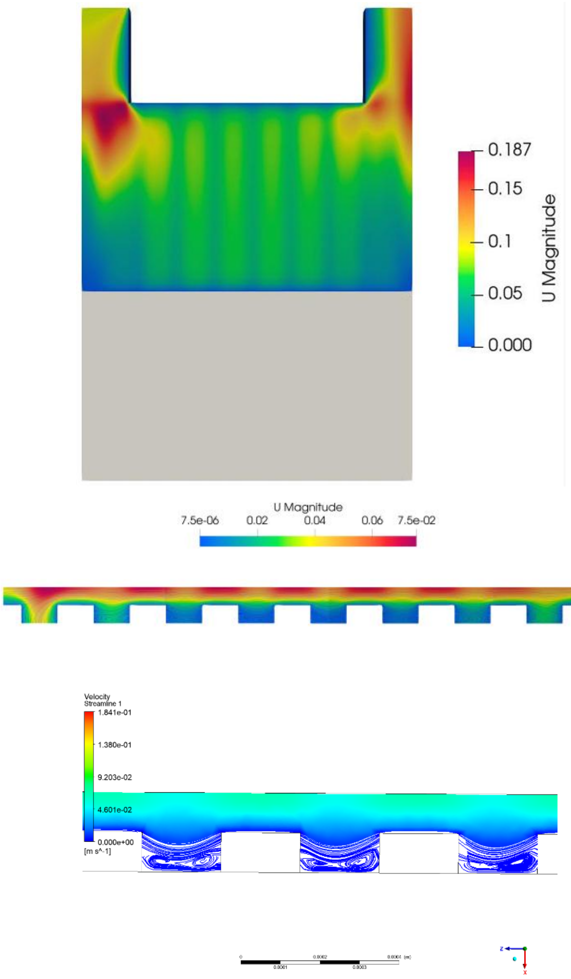

Fig. 7. Velocity magnitude and streamlines for the base case showing recirculating wakes.

C. Cut Square Pins

The cut square pin configuration introduces material removal from the pin body, reducing the solid cross-section. This modification yields an HTC of 25,695 W/m²K with a heater surface temperature of 327.32 K and a pressure drop of 126.19 Pa. The pumping power is 0.001583 mW/mm². Compared to the base case, the HTC decreases by 14.2%, the largest thermal penalty observed among the pin-shape modifications. This significant reduction is attributed to the loss of wetted surface area and conductive cross-section: the removed material reduces both the fin efficiency and the available area for convective heat exchange. However, the pressure drop decreases by 3.8%, offering a modest hydraulic benefit. The cut pin configuration is therefore not recommended where thermal performance is the primary design objective.

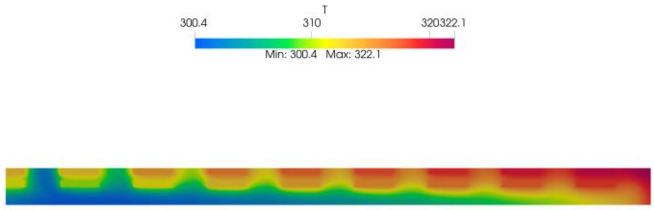

Fig. 8. Mid-plane temperature distribution for the cut square pin configuration.

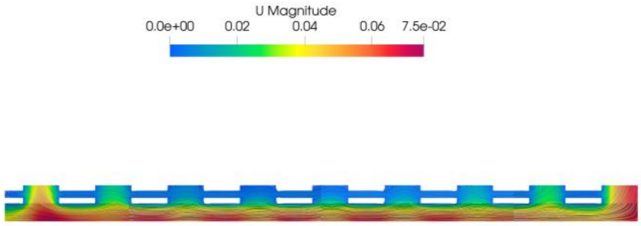

Fig. 9. Mid-plane streamlines for the cut square pin configuration.

D. Filleted Square Pins

The filleted square pin configuration introduces fillet radii at the pin root, smoothing the transition between the pin and the base plate. This modification achieves an HTC of 29,425 W/m²K with a heater surface temperature of 324.24 K and a pressure drop of 123.11 Pa. The pumping power is 0.001544 mW/mm². The HTC decreases by only 1.8% relative to the base case, while the pressure drop decreases by 6.2%, demonstrating that the fillet effectively streamlines the near-root flow, shrinking the horseshoe vortex at the fin leading edge and reducing form drag. The thermal penalty is modest because the fillet adds conductive material at the root, partially compensating for the reduced vortical mixing. The filleted configuration represents an attractive design option where a modest hydraulic improvement is desired with minimal thermal compromise.

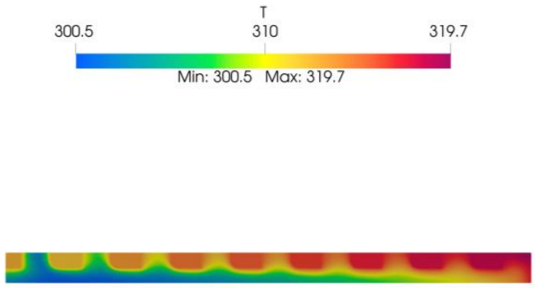

Fig. 10. Mid-plane temperature distribution for the filleted square pin configuration.

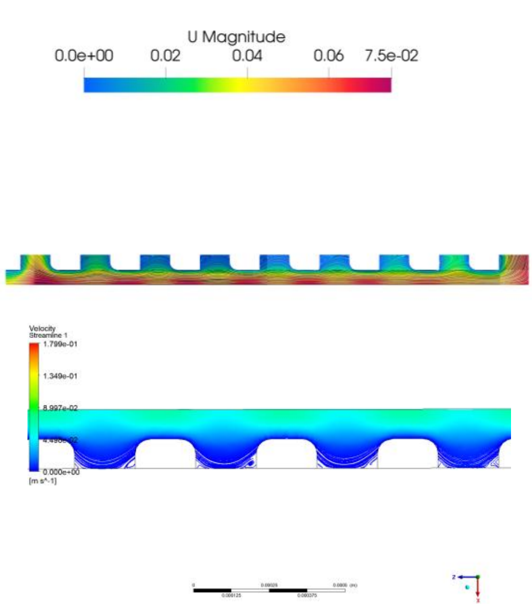

Fig. 11. Mid-plane streamlines for the filleted square pin configuration.

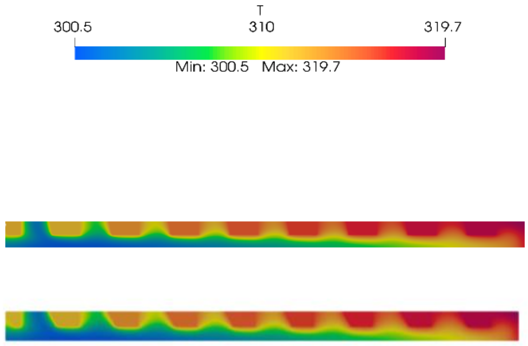

Fig. 12. Mid-plane temperature distribution for the 10% and 30% chamfer configuration.

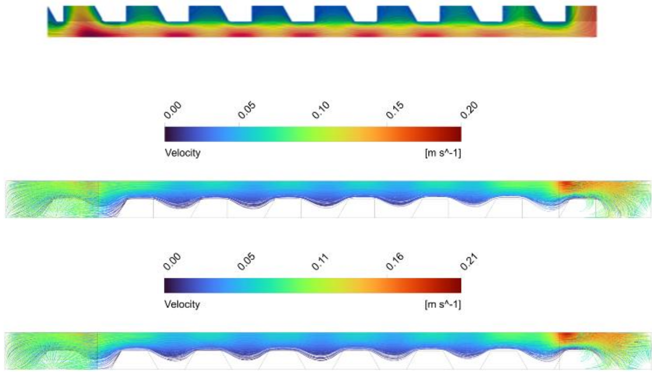

Fig. 13. Mid-plane streamlines for the 30% chamfer configuration.

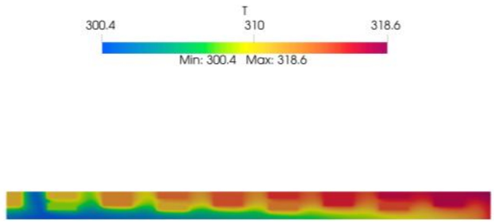

Fig. 14. Mid-plane temperature distribution for the aspect-ratio + cut-through configuration.

E. Chamfer Study (10%, 20%, 30%)

The chamfer study examines the effect of progressively chamfering the corners of the square pins at 10%, 20%, and 30% levels. As the chamfer increases, the pin cross-section transitions from a sharp-cornered square toward an octagonal profile, reducing the frontal area and rounding the flow separation points.

The 10% chamfer achieves an HTC of 29,366 W/m²K at a pressure drop of 125.04 Pa (pumping power: 0.001568 mW/mm²), representing a 1.9% reduction in HTC and a 4.7% reduction in pumping power relative to the base case. The 20% chamfer yields an HTC of 28,742 W/m²K at a pressure drop of 118.83 Pa (pumping power: 0.001490 mW/mm²), with a 4.0% HTC reduction and a 9.4% pumping power reduction. The 30% chamfer achieves an HTC of 28,015 W/m²K at a pressure drop of 111.79 Pa (pumping power: 0.001402 mW/mm²), with a 6.5% HTC reduction and a 14.8% pumping power reduction.

The trend is clear and monotonic: increasing the chamfer progressively reduces both the thermal and hydraulic performance. The hydraulic benefit exceeds the thermal penalty at each level — the 30% chamfer saves nearly 15% of the pumping power at a 6.5% thermal cost — making chamfered pins an efficient strategy for designs constrained by pumping budget. The heater surface temperature rises progressively from 324.28 K (10%) to 324.75 K (20%) to 325.31 K (30%), confirming the thermal trade-off. The mechanism is analogous to that of the fillet: the chamfer reduces the sharp-corner stagnation and wake recirculation that contribute to both flow resistance and local mixing enhancement.

TABLE IV. Effect of Pin Chamfer on Thermo-Hydraulic Performance

Configuration	h [W/m² K]	Δh vs. Base	ΔP [Pa]	P_mech [mW/mm²]	ΔP_mech vs. Base	T_heater [K]
Base Case (Square Pins)	29,950	—	131	0.001646	—	323.9
Chamfer 10%	29,366	-1.9%	125	0.001568	-4.7%	324.3
Chamfer 20%	28,742	-4.0%	119	0.001490	-9.5%	324.7
Chamfer 30%	28,015	-6.5%	113	0.001402	-14.8%	325.3

F. *Aspect Ratio Modification with Cut-Through Holes*

This configuration combines a modified pin aspect ratio with transverse cut-through holes, aiming to simultaneously enlarge the wetted surface and reduce flow blockage. It achieves an HTC of 31,481 W/m²K with a heater surface temperature of 322.85 K and a pressure drop of 194.33 Pa. The pumping power is 0.002437 mW/mm².

Compared to the base case, this configuration delivers a 5.1% improvement in HTC, making it the second-best thermal performer after the novel design. However, the pressure drop increases by 48.1% relative to the base case, and the pumping power rises by 48.1%. The cut-through holes allow a fraction of the flow to pass through the pin body, sustaining local mixing in the pin wake while the elongated aspect ratio increases the wetted surface for convection. The trade-off is favorable for applications where a moderate increase in pumping power is acceptable in exchange for a meaningful thermal improvement.

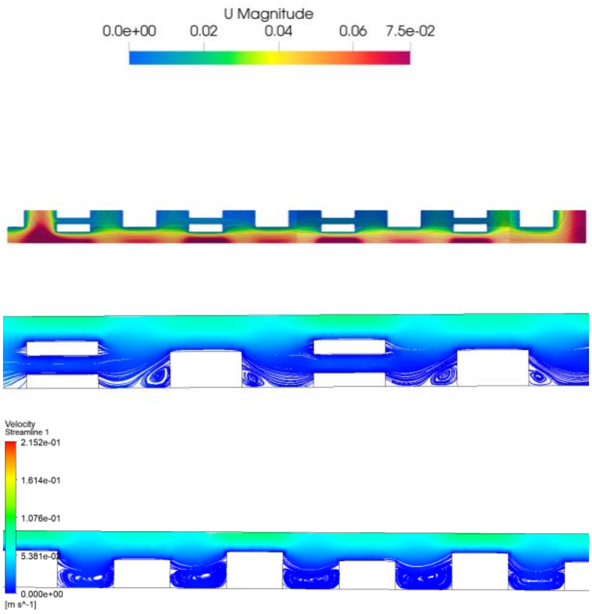

Fig. 15. Mid-plane streamlines for the aspect-ratio + cut-through configuration.

G. *Novel Design (Aspect ratio + cut fins optimized)*

The novel design represents the most aggressive geometric modification in this study, combining multiple enhancement strategies to maximize thermal performance. It achieves a remarkable HTC of 41,975 W/m²K, the highest among all configurations, with a heater surface temperature of 317.89 K, the lowest recorded in the study. The pressure drop is 1296.01 Pa and the pumping power is 0.016253 mW/mm².

Compared to the base case, the HTC improves by 40.2%, a substantial enhancement that reflects the combined effect of enhanced flow mixing, increased wetted surface area, and intensified boundary layer disruption. The heater surface temperature drops from 323.87 K to 317.89 K, a reduction of 5.98 K, which can be critical for ensuring the junction temperature of high-power electronics remains within safe operating limits.

However, this exceptional thermal performance comes at a significant hydraulic cost: the pumping power increases by approximately 888% relative to the base case. The pressure drop of 1296.01 Pa is approximately 10 times that of the base case, indicating that the geometric modifications create substantial flow blockage and recirculation. This configuration is therefore recommended only for applications where thermal dissipation is the overriding constraint and the system can accommodate the elevated pumping requirements.

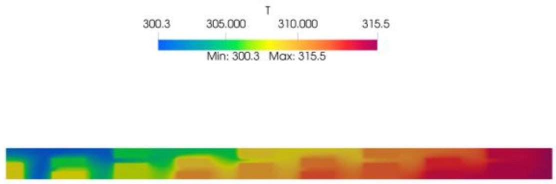

*Fig. 16. Mid-plane temperature distribution for the novel design (*Aspect ratio + cut fins optimized*).*

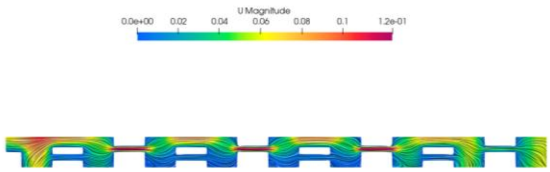

*Fig. 17. Mid-plane streamlines for the novel design (*Aspect ratio + cut fins optimized*).*

H. *Fin Removal Strategy*

The fin removal strategy investigates the effect of selectively removing fins from the array to reduce flow blockage and lower the pressure drop. This configuration achieves an HTC of 28,052 W/m²K with a heater surface temperature of 325.28 K and a pressure drop of 118.10 Pa. The pumping power is 0.001493 mW/mm².

The HTC decreases by 6.3% relative to the base case, which is expected since fewer fins mean less wetted surface area and fewer flow interruptions to restart the thermal boundary layer. The pumping power, however, decreases by 9.2%, providing a net hydraulic benefit. The thermal-to-hydraulic trade-off ratio (approximately 0.69) is less favorable than the chamfer strategy (where the 30% chamfer achieves a ratio of 0.44), suggesting that selective chamfering is a more efficient approach to hydraulic relief than fin removal. The fin removal strategy may be considered in combination with other modifications as part of a multi-objective optimisation.

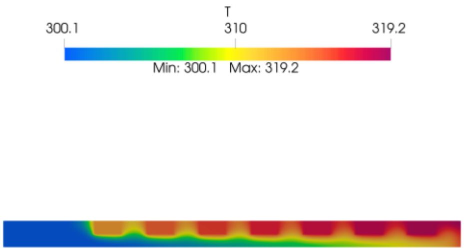

Fig. 18. Mid-plane temperature distribution for the fin removal configuration.

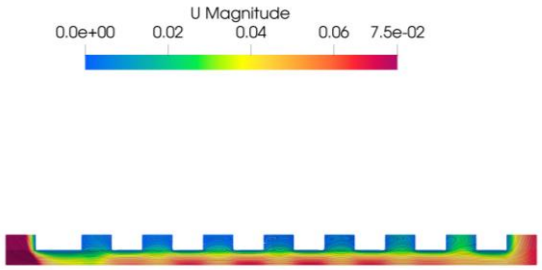

Fig. 19. Mid-plane streamlines for the fin removal configuration.

VI. Overall Comparison

Table VI consolidates the thermo-hydraulic performance of all eleven configurations investigated in this study. The data enables a direct comparison of the thermal effectiveness and hydraulic cost of each geometric modification relative to the base case.

TABLE V. Summary of All Investigated Configurations

Configuration	h [W/m²K]	Δh vs. Base	P_mech [mW/mm²]	ΔP_mech vs. Base
Single Inlet	32,740	+9.3%	0.0216	+1214.8 %
Five Inlets (no pins)	33,133	+10.6 %	0.0029	+76.7%
Five Inlets + Square Pins (Base)	29,950	—	0.001646	—
Cut Square Pins	25,695	-14.2%	0.001583	-3.8%
Filleted Square Pins	29,425	-1.8%	0.001544	-6.2%
Chamfer 10%	29,366	-1.9%	0.001568	-4.7%
Chamfer 20%	28,742	-4.0%	0.001490	-9.5%
Chamfer 30%	28,015	-6.5%	0.001402	-14.8%
Aspect Ratio + Cut	31,481	+5.1%	0.002437	+48.1%
Novel 1	41,975	+40.2 %	0.016253	+887.7%
Fin Removal	28,052	-6.3%	0.001493	-9.3%

The results reveal several important trends. First, modifications that reduce the pin cross-section or remove material (chamfers, cuts, fin removal) consistently reduce both HTC and pumping power, with the hydraulic benefit typically exceeding the thermal penalty. Second, modifications that increase flow blockage or enhance mixing (aspect ratio + cut, Novel) improve the HTC but at a hydraulic cost that grows faster than the thermal gain. Third, the five-inlet manifold design is highly effective at reducing the overall pressure drop compared to a single-inlet design, even when pin fins are added.

Among the configurations studied, the chamfer series offers the most predictable and controllable trade-off: each 10% increment of chamfer yields approximately 2% HTC reduction with approximately 5% pumping power savings. The filleted pin configuration achieves a similar trade-off but through a different mechanism (root smoothing vs. corner rounding). The aspect-ratio + cut configuration is the best option for thermal improvement at moderate hydraulic cost (+5.1% HTC at +48.1% pumping power). The Novel design delivers the highest absolute HTC (41,975 W/m²K) but at a pumping power approximately 10 times that of the base case.

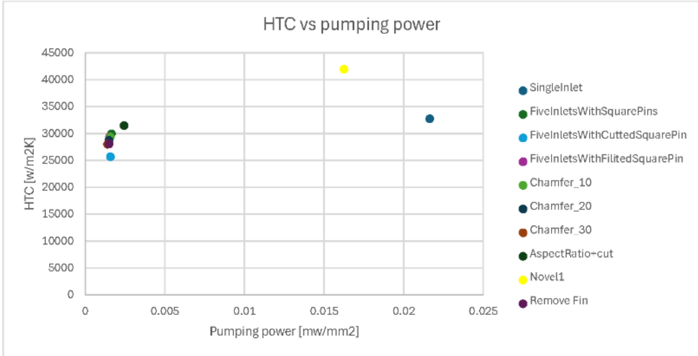

Fig. 20. Performance map: HTC vs. pumping power for all configurations

VII. Conclusions

A comprehensive three-dimensional conjugate heat-transfer CFD investigation of eleven geometric configurations of a microchannel heat sink with pin fins was performed. The following conclusions are drawn:

1) The five-inlet manifold design is highly effective at reducing pressure drop. Compared to a single-inlet design, the five-inlet configuration reduces the pumping power by 86.6% while maintaining comparable HTC, demonstrating that manifold-level flow management is as important as pin-level geometry optimisation.

2) The base case (five-inlet with square pins) achieves an HTC of 29,950 W/m²K at a pumping power of 0.001646 mW/mm². The sharp corners of the square pins generate stagnation zones and recirculating wakes that simultaneously enhance mixing and increase form drag.

3) Pin chamfering provides a predictable, monotonic trade-off between thermal and hydraulic performance. The 30% chamfer reduces pumping power by 14.8% at a 6.5% HTC cost, making it the most energy-efficient pin-level modification. This represents a favorable thermal-to-hydraulic penalty ratio of 0.44.

4) The filleted pin configuration achieves a similar benefit to chamfering (−1.8% HTC, −6.2% pumping power) through root smoothing rather than corner modification, and may be preferred for manufacturing compatibility.

5) Cutting material from the pin body is counterproductive: the 14.2% HTC reduction is disproportionate to the modest 3.8% hydraulic benefit, as the removed material significantly reduces both the wetted surface and the conductive path.

6) The aspect-ratio modification with cut-through holes delivers a 5.1% HTC improvement at a 48.1% pumping power increase, offering a viable option for designs with adequate pumping budget that prioritize thermal performance.

7) The novel design (Aspect ratio + cut fins optimized) achieves the highest HTC of 41,975 W/m²K, a 40.2% improvement over the base case, with the lowest heater temperature of 317.89 K. However, the ~888% increase in pumping power limits its applicability to scenarios where thermal dissipation is the critical constraint.

8) Selective fin removal provides a 9.2% pumping power reduction at a 6.3% HTC cost, a less favorable ratio than chamfering, suggesting that material redistribution (chamfering) is preferable to material elimination (fin removal).

Future work will address the following limitations: (i) a formal multi-objective optimisation over the combined parameter space to capture interactions between geometric modifications and identify global optima and (iv) experimental validation on a fabricated prototype to confirm the numerical predictions.

REFERENCES

[1] G. E. Moore, "Cramming more components onto integrated circuits," Electronics, vol. 38, no. 8, pp. 114-117, 1965.

[2] S. M. S. Murshed, "Introductory chapter: Electronics cooling—An overview," in Electronics Cooling, IntechOpen, 2016, doi: 10.5772/63321.

[3] Z. Zhang, X. Wang, and Y. Yan, "A review of the state-of-the-art in electronic cooling," e-Prime, vol. 1, p. 100009, 2021, doi: 10.1016/j.prime.2021.100009.

[4] J. R. Black, "Electromigration—A brief survey and some recent results," IEEE Trans. Electron Devices, vol. 16, no. 4, pp. 338-347, 1969, doi: 10.1109/T-ED.1969.16754.

[5] X. Nie, C. Zhu, T. Fu, and Y. Ma, "Mass transfer intensification and mechanism analysis of gas-liquid two-phase flow in the microchannel embedding triangular obstacles," Chin. J. Chem. Eng., vol. 51, pp. 100-108, 2022.

[6] D. B. Tuckerman and R. F. W. Pease, "High-performance heat sinking for VLSI," IEEE Electron Device Lett., vol. 2, no. 5, pp. 126-129, 1981, doi: 10.1109/EDL.1981.25367.

[7] Y. Alihosseini, M. Zabetian Targhi, M. M. Heyhat, and N. Ghorbani, "Effect of a micro heat sink geometric design on thermo-hydraulic performance: A review," Appl. Therm. Eng., vol. 170, p. 114974, 2020, doi: 10.1016/j.applthermaleng.2020.114974.

[8] T. Alam and M. H. Kim, "A comprehensive review on single phase heat transfer enhancement techniques in heat exchanger applications," Renew. Sustain. Energy Rev., vol. 81, pp. 813-839, 2018, doi: 10.1016/j.rser.2017.08.060.

[9] M. H. Mousa, N. Miljkovic, and K. Nawaz, "Review of heat transfer enhancement techniques for single phase flows," Renew. Sustain. Energy Rev., vol. 137, p. 110566, 2021, doi: 10.1016/j.rser.2020.110566.

[10] M. P. Vasilev, R. S. Abiev, and R. Kumar, "Effect of circular pin-fins geometry and their arrangement on heat transfer performance for laminar flow in microchannel heat sink," Int. J. Therm. Sci., vol. 170, p. 107177, 2021.

[11] M. A. Alfellag, H. E. Ahmed, O. T. Fadhil, and A. Sh. Kherbeet, "Optimal hydrothermal design of microchannel heat sink using trapezoidal cavities and solid/slotted oval pins," Appl. Therm. Eng., vol. 158, p. 113765, 2019, doi: 10.1016/j.applthermaleng.2019.113765.

[12] J. Hua, G. Li, X. Zhao, Q. Li, and J. Hu, "Study on the flow resistance performance of fluid cross various shapes of micro-scale pin fin," Appl. Therm. Eng., vol. 107, pp. 768-775, 2016, doi: 10.1016/j.applthermaleng.2016.07.048.

[13] P. Bhandari and Y. K. Prajapati, "Thermal performance of open microchannel heat sink with variable pin fin height," Int. J. Therm. Sci., vol. 159, p. 106609, 2021, doi: 10.1016/j.ijthermalsci.2020.106609.

[14] J. Xie, H. Yan, B. Sunden, and G. Xie, "The influences of sidewall proximity on flow and thermal performance of a microchannel with large-row pin-fins," Int. J. Therm. Sci., vol. 140, pp. 8-19, 2019, doi: 10.1016/j.ijthermalsci.2019.02.031.

[15] K. Fu, W. Gao, X. Xu, and X. Liang, "Flow boiling heat transfer and pressure drop characteristics of water in a copper foam fin microchannel heat sink," Appl. Therm. Eng., vol. 218, p. 119295, 2023, doi: 10.1016/j.applthermaleng.2022.119295.

[16] K. Derakhshanpour, R. Kamali, and M. Eslami, "Effect of rib shape and fillet radius on thermal-hydrodynamic performance of microchannel heat sinks: A CFD study," Int. Commun. Heat Mass Transf., vol. 119, p. 104928, 2020.

[17] A. Manoj, U. V. Goddumarri, R. A., and S. Chakraborty, "Heat transfer and fluid flow characteristics of a microchannel heat sink with microplates—A critical computational study," Appl. Therm. Eng., vol. 226, p. 120309, 2023.

[18] K. N. Ramesh, T. K. Sharma, and G. A. P. Rao, "Latest advancements in heat transfer enhancement in the micro-channel heat sinks: A review," Arch. Comput. Methods Eng., vol. 28, pp. 3115-3134, 2021.